forests

MDPI

Article

Influence of Root Distribution on Preferential Flow in Deciduous and Coniferous Forest Soils

Ziteng Luo [1,2], Jianzhi Niu [1,2,*], Baoyuan Xie [1], Linus Zhang [3], Xiongwen Chen [4,5], Ronny Berndtsson [3], Jie Du [1], Jiakun Ao [1], Lan Yang [1] and Siyu Zhu [1]

1 Key Laboratory of State Forestry Administration on Soil and Water Conservation, Beijing Engineering Research Center of Soil and Water Conservation, Engineering Research Centre of Forestry Ecological Engineering, Ministry of Education, School of Soil and Water Conservation, Beijing Forestry University, Beijing 100083, China; xjzitengluo@163.com (Z.L.); xie4412@sina.com (B.X.); taiyuandujie1992@163.com (J.D.); ajk7777777@163.com (J.A.); a18404982617@163.com (L.Y.); zhusiyu2017@126.com (S.Z.)
2 Beijing Collaborative Innovation Center for Eco-Environmental Improvement with Forestry and Fruit Trees, Beijing 102206, China
3 Department of Water Resources Engineering & Center for Middle Eastern Studies, Lund University, Box 118, SE-221 00 Lund, Sweden; Linus.zhang@tvrl.lth.se (L.Z.); ronny.berndtsson@tvrl.lth.se (R.B.)
4 Department of Biological and Environmental Sciences, Alabama A&M University, Normal, AL 35762, USA; xchen.aamu@gmail.com
5 Jiyang College, Zhuji 311800, Zhejiang Province, China
* Correspondence: nexk@bjfu.edu.cn; Tel.: +86-10-5168-7338

Received: 27 August 2019; Accepted: 1 November 2019; Published: 5 November 2019

Abstract: Root-induced channels are the primary controlling factors for rapid movement of water and solute in forest soils. To explore the effects of root distribution on preferential flow during rainfall events, deciduous (*Quercus variabilis* BI.) and coniferous forest (*Platycladus orientalis* (L.) Franco) sites were selected to conduct dual-tracer experiments (Brilliant Blue FCF and Bromide [Br^-]). Each plot (1.30 × 1.30 m) was divided into two subplots (0.65 × 1.30 m), and two rainfall simulations (40 mm, large rainfall and 70 mm, extreme rainfall) were conducted in these. Vertical soil profiles (1.00 m × 0.40 m) were excavated, and preferential flow path features were quantified based on digital image analysis. Root (fine and coarse) abundance and Br^- concentration were investigated for each soil profile. In deciduous forest, accumulated roots in the upper soil layer induce larger lateral preferential flow as compared to the coniferous forest soil during large rainfall events. Compared with deciduous forest, coniferous forest soil, with higher (horizontal and vertical) spatial variability of preferential flow paths, promotes higher percolation and solute leaching to deeper soil layers during extreme rainfall events. Fine roots, accounting for a larger proportion of total roots (compared to coarse roots), facilitate preferential flow in the 0–40 cm forest soil layer. Overall, our results indicate that the root distribution pattern of different tree species can exert diverse effects on preferential flow in forest soils.

Keywords: preferential flow; dual-tracer experiment; root distribution; solute leaching; tree species

1. Introduction

Preferential flow, without conforming to Darcy's flow, is well recognized as a potentially important mechanism in soils [1–3]. This kind of flow can increase the leaching potential of soils and limit the storage, filter, and buffer functions of soils, and associate with a large number of inaccuracies in water and solute transport predictions [4–10]. Continuous root channels can generate preferential flow paths, and promote movement of water and solutes with little resistance [11–15]. Thus, hydrological and mass transport processes below the root zone are likely to be influenced by root systems in structured soils [16]. In the entire soil layer, root channels (living and dead) can account for 70–100% of the total macropore population [17,18]. Soil profiles with large amounts of roots can thus, induce more water and solute preferential movement [19,20]. Generally, fine and coarse roots can form permanent channels for preferential flow with different mechanisms [21]. For fine roots, the rhizosphere exudates associated with microorganisms and plant fine roots can increase organic matter, which subsequently supports soil aggregation and the formation of inter-aggregate macropores [22,23]. Large amounts of well-connected fine roots can form complex networks and enhance the rapid movement of water and solute [24]. Additionally, the presence of fine roots is closely associated with the increase of noncapillary porosity and infiltration capacity [11]. In field experiments, higher fine root length density and larger biomass are usually found in preferential flow paths as compared to the soil matrix [25]. Furthermore, positive correlation between fine roots and soil water content resulting from preferential flow has been observed in forest soils [26]. On the other hand, physical processes around coarse roots can expand the diameter of root channels [21,27]. Laterally-oriented coarse roots can lead fast and downslope lateral flow [28]. However, restricted by difficulties in using non-destructive methods, there is still little scientific understanding of the impacts of root distribution on the preferential transport of water and solutes.

In view of the above, forest soils require particular attention [29,30] mainly because of the presence of well-developed aggregates and soil pore structures that are rarely disturbed [3]. Preferential paths in forest soils can last for decades or more, and may be continuous from the surface to deeper soil horizons [3,31,32]. In forest soils, root channels are the primary preferential paths for water and solute transport [33–36]. Thus, preferential flow in forest soils is closely related to nutrient leaching, soil erosion, and safe groundwater access [31,37]. In northern China, deciduous and coniferous forests are widely planted for the purpose of soil and water conservation. Different root distribution patterns are found for these two types of forests. Abundant roots accumulate in shallower soil layers of deciduous forest, whereas roots are mainly observed in deeper soil layers for coniferous forest [38–40]. There has been little quantitative analysis of different effects of fine and coarse roots on preferential flow in deciduous and coniferous forests. Moreover, approximately 70–80% of precipitation occurs during the rainy season (June-September) in northern China [41]. High-intensive rainfall events are common during the rainy season in this area [41]. This creates problems for the management of water conservation forest ecosystems [42]. Previous studies have shown that the soil structure is the critical factor for preferential flow during large and high-intensive rainfall events [43]. Therefore, it is important to characterize the features of roots (fine and coarse) enhanced preferential flow in deciduous and coniferous forests soils for this type of rainfall events.

Preferential flow paths can be visualized by dye tracer experiments. Dye tracer experiments have been widely used to study the preferential flow pattern, often with Brilliant Blue FCF, a common, nontoxic, and inexpensive tracer [16,44–46]. Anion Br^- with high solubility, small molecular size, and low reactivity can be used as proxy to observe the leaching of water, salts, and nutrients in field studies [16,47,48]. Therefore, experiments using two kinds of tracers (Brilliant Blue and Br^-) can obtain more important features of water and solute movement as compared to a single tracer [16,44].

In the present study, two typical and widely distributed forests (i.e., a deciduous forest dominated by *Quercus variabilis* BI., and a coniferous forest mainly planted with *Platycladus orientalis* (L.) Franco were selected to conduct dual-tracer experiments (Brilliant Blue and Br^-). Rainfall simulations corresponding to 40 mm (large rainfall event), and 70 mm (extreme rainfall event) were used in the experiments. Abundance and size of roots (fine and coarse) were investigated for the soil profiles. The objectives of this paper were: (1) to characterize features of preferential flow paths in deciduous forest (DF) and coniferous forest (CF) soils under simulated rainfall events; (2) to explore the effects of fine and coarse roots on preferential flow.

2. Materials and Methods

2.1. Study Area

This study was conducted at the Jiufeng Forest Ecosystem Research Station (40°03′54″ N, 116°05′45″ E, 811.173 hm^2) located northwest of Beijing, China. The research station is primarily used for education and research. It is located in a typical continental warm temperate zone with a monsoon climate. Annual precipitation is about 660 mm of which 70–80% occur during the rainy season (June–September) [41]. Annual average temperature is 12.5 °C. The majority of existing forests in Mount Jiufeng was planted in the 1950s and 1960s, and the percentage of vegetation cover is approximately 86%. Overstory tree species in the entire mountain area are primarily 17.3% *Platycladus orientalis* (L.) Franco, 19.1% *Pinus tabulaeformis* Carr., 26.2% *Quercus variabilis* BI., and 3.9% *Robinia pseudoacacia* [39,49]. Two typical deciduous forests (DF) and coniferous forest (CF) sites dominated by either *Quercus variabilis* Bl. or *Platycladus orientalis* (L.) Franco were selected in the present study. The soil texture at the study sites is sandy loam, and the undergrowth vegetation at each site is healthy and undamaged [44]. At each site, each plot was divided into two subplots to conduct dye and tracer experiments. Rainfall equivalent to 40 and 70 mm was applied to each subplot. The two plots were located at about 255 and 275 m amsl, respectively, in a flat semi-sunny area (Table 1). Near each plot, intact soil cores of 200 cm^3 were collected at four depth intervals (0–10, 10–20, 20–30, and 30–40 cm) to measure bulk density. For each soil layer, four replicate soil cores were prepared at each site. Disturbed soil samples were taken from each soil interval (0–10, 10–20, 20–30, and 30–40 cm) at four random locations at each site to estimate initial soil water content. Soil samples from the same soil intervals were mixed up and dried at 105 °C for 24 h to obtain initial soil water content. Physicochemical properties of the soils are presented in Table 1. All field experiments were conducted in August 2018.

Table 1. Characteristics of the two experimental study sites and soil physicochemical properties in the 0–40 cm soil layer.

Forest Type	Dominant Tree Species	Geographic Position	Altitude (m)	Aspect	Soil Layer (cm)	ISWC (%)	BD (g/cm^3)	SOC (%)
DF	*Quercus variabilis* Bl.	40°3′41″ N 115°5′29″ E	275	East 32.5° to south	0–10	10.7	1.32 ± 0.06	4.1
					10–20	8.3	1.38 ± 0.15	1.8
					20–30	8.2	1.42 ± 0.04	2.0
					30–40	10.8	1.37 ± 0.08	0.8
CF	*Platycladus orientalis* (L.) Franco	40°3′42″ N 115°5′373″ E	255	East 19.5° to south	0–10	12.7	1.21 ± 0.13	5.8
					10–20	14.1	1.24 ± 0.13	3.7
					20–30	12.5	1.23 ± 0.10	2.2
					30–40	12.6	1.18 ± 0.13	2.7

DF: deciduous forest; CF: coniferous forest; ISWC: initial soil water content; BD: bulk density; SOC: soil organic carbon.

2.2. Tracer Experiment

At each site, each plot was located at a similar distance from the tree stems. The plots were surrounded by square steel frames (130 × 130 cm^2), inserted into the soil to a depth of 15 cm. Fresh fallen leaves were removed without disturbing the humus layer [44]. Before performing the tracer experiment, each plot was divided into two small subplots (65 × 130 cm^2) for the different rainfall application amounts (40 and 70 mm) (Figure 1). In total, 93 L mixed solution containing Brilliant Blue (5 g/L) and Br^- (10 g/L) was uniformly sprinkled onto each plot with a rechargeable backpack sprayer. A sprinkle rate of 50 mm/h was selected to ensure that no obvious ponding would occur during entire dye experiments [44]. During the first 48 min both subplots were sprinkled simultaneously. Then, one subplot was covered with a plastic sheet to protect the area from further tracer application. Immediately after this, the other subplot was sprinkled during another 36 min until the application amount of 70 mm was reached (Figure 1). Afterwards, both subplots were covered by a plastic sheet (2 × 2 m^2) to prevent evaporation and rainfall infiltration [1,16,50]. Each subplot was left for 24 h to complete the infiltration process [1,45]. The DF-40 mm and CF-40 mm denote the dye experiments conducted with 40 mm rainfall for the DF and CF, respectively. The DF-70 mm and CF-70 mm denote dye experiments performed with 70 mm rainfall for DF and CF, respectively.

After 24 h, the plastic sheet and steel frame were carefully removed. Firstly, the subplots (130×60 cm^2) for the 40 mm rainfall were excavated vertically in 5 cm intervals to a depth of 40 cm as constrained by the maximum dye-stained depth and bedrock location (Figure 1). The size of each vertical profile was 100×40 cm^2. To avoid boundary effects, vertical profiles were sequentially confined at 5 cm from the edge of the frame in each subplot. Thus, 8 vertical profiles were obtained with a lateral increment of 5 cm for the further dye pattern analysis in each subplot (Figure 1). After that, the 70 mm rainfall subplots (130×60 cm^2) were excavated vertically in 5 cm intervals, as well to a depth of 40 cm. After excavation, the profile edges were marked using rulers for further distortion correction. Next, each vertical profile layer was photographed by a digital camera (Sony ILCE-*a*6000, Sony, Tokyo, Japan).

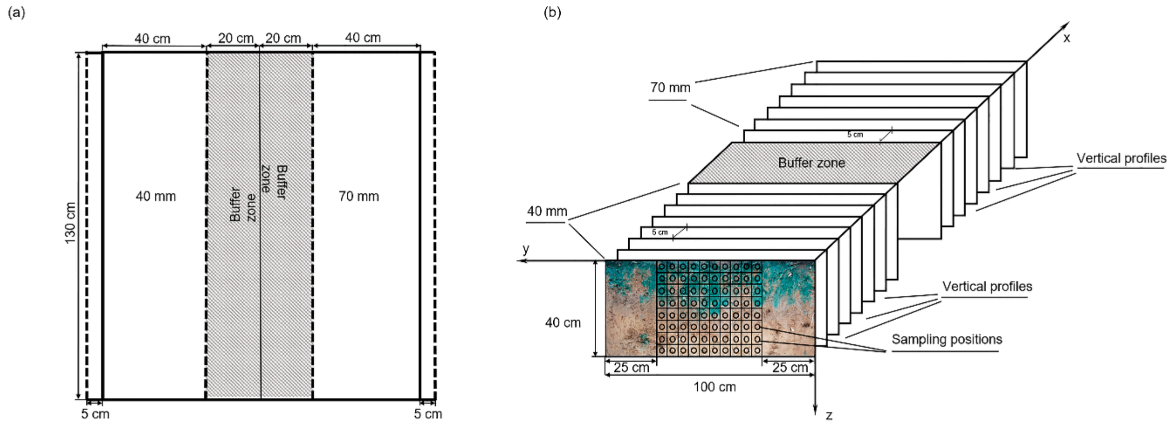

Figure 1. (**a**) Experimental set-up seen from above, (**b**) vertical soil profile excavation, and soil sample collection.

2.3. Root Abundance (RA) Investigating

After images of soil profiles were taken, the distribution patterns of roots in vertical and horizontal for the entire soil profile (100×40 cm^2) were investigated by using a 5×5 cm grid system (Figure 1). Roots were sorted into two classes ($0 <$ diameter ≤ 5 mm, and diameter > 5 mm) by calipers at the points close to the visible soil surface profiles. Roots with diameter ≤ 5 mm were defined as fine, and roots with diameter > 5 mm were classified as coarse [51,52]. The number of roots in each class and every grid was used in the calculation of root abundance (*RA*) (number/dm^2) following a similar methodology as suggested by van Noordwijk et al. and Vanlauwe et al. [53,54]. In our study, the *RA* of 16 soil profiles for each plot was averaged to represent the root distribution pattern of each site.

2.4. Soil Sample Collection for Solute Concentration

Soil samples were obtained from the soil profiles determining the concentration of Br^-. A gridded frame (50 cm by 40 cm) consisting of 80 small grids (5 cm by 5 cm) was put at 25 cm from the left and right edges of each soil profile (Figure 1). Approximately 70 g soil were collected from each grid and used to determine Br^- concentration using ion meter (PXSJ-216F, Shanghai INESA & Scientific Instrument Co., Ltd., Shanghai, China). The detailed procedure is described by Luo et al. [44].

2.5. Flow Classification and Dye Pattern Analysis

After geometric correction, each soil profile image was classified into dye stained or unstained using Adobe Photoshop CS6 (Adobe Systems Inc., San Jose, CA, USA) [55,56]. Black areas thus represented stained paths, while white areas indicated unstained areas. The resolution was set to

100 pixels per cm^2 for all profile images. The dye coverage (DC) was calculated according to the percentage of black pixels in each horizontal line in the binary images for each vertical profile. In total, the DC of 16 vertical soil profiles was obtained from each plot. The flow types in the vertical soil profiles were classified according to Weiler and Fluhler [57], and described in detail in Table 2.

Table 2. Definition of flow type according to stained pathway width and dye coverage [57].

Flow Type	Dye Coverage (DC) of Stained Pathway Width for <20 mm	>200 mm
Macropore flow with low interaction	>50%	<20%
Macropore flow with mixed interaction	20–50%	<20%
Macropore flow with high interaction	<20%	<30%
Heterogeneous matrix flow and fingering	<20%	30–60%
Homogeneous matrix flow	<20%	>60%

To compare the spatial variation of preferential flow paths between DF and CF, mean DC data for each plot were tested for normality by the Kolmogorov-Smirnov test at 0.05 significance level. Data sets that did not pass the normal distribution test were transformed by Johnson transformation using the Minitab 15.0 statistical software (Minitab Inc., State College, PA, USA), and arcsine square root transformation [58]. Data following normal distribution were analyzed using the GS+ geostatistics software (Version 9.0, Gamma Design Software 2000) [59,60] for the spatial variation of preferential pathways in the vertical and horizontal direction. Experimental semivariograms γ were estimated using the following equation:

$$\gamma(l) = \frac{1}{2N(l)} \sum_{i=1}^{N(l)} [A_i(x_i) - A_i(x_i + l)]^2 \tag{1}$$

where $N(l)$ is the number of observed pairs separated by lag distance l; $A_i(x_i)$ and $A_i(x_i + l)$ are the mean DC values at x_i and $x_i + l$, respectively. These locations were defined as the center of each 5×5 cm^2 squares in the binary images [55,61]. An exponential model was fitted to the experimental semivariograms in horizontal direction according to:

$$\gamma(l) = \begin{cases} 0, & l = 0 \\ C_0 + C\left(1 - e^{-\frac{l}{a}}\right), & l > 0 \end{cases} \tag{2}$$

The gaussian model was fitted to the experimental semivariograms in vertical direction according to:

$$\gamma(l) = C_0 + C\left[1 - \exp\left(\frac{-l^2}{a^2}\right)\right] \tag{3}$$

Here, C_0 and $C_0 + C$ are the nugget and sill, respectively, when $l = 3a$, $1 - \exp^{-\frac{h}{a}} = 1 - \exp^{-3} \approx 1$, and $\gamma(l) \approx C_0 + C$. Therefore, the range of the semivariogram for exponential and gaussian models is $3a$ and $\sqrt{3}a$ [62,63], respectively. The semivariogram model was selected so that the coefficient of determination was maximized and the residual sum of squares, range, and nugget was minimized.

2.6. Root-Solute Interaction (RSI)

Relative Br^- concentration (C, %) was calculated [44,61] and combined with RA to obtain the RSI for soil profiles:

$$RSI = RA\frac{C - C_{\min}}{C_{\max} - C_{\min}} \tag{4}$$

where RA (number/dm^2) and C are the total root abundance and the Br^- concentration (mg/(kg soil)) in soil samples collected in the 5 by 5 cm grid. C_{max} and C_{min} are maximum and minimum Br^- concentration (mg/(kg soil) in each soil profile, respectively.

3. Results

3.1. Observed Preferential Flow Paths

The pattern of preferential flow paths indicated a difference between DF and CF under large (40 mm) and extreme (70 mm) rainfall events (Figure 2). The DC decreased with soil depth for both DF and CF. In the upper 0–10 cm soil layer, the stained regions were more homogeneous than for deeper soil layers, which was more obvious at the DF site. Additionally, the number of stained preferential paths was larger at the DF than at the CF site (Figure 2). Generally, the DC was larger under extreme rainfall as compared to the large rainfall at both sites and every soil layer. Compared to the DC of CF-40 mm, the DC of CF-70 mm was significantly larger for each soil layer ($p < 0.05$). Mean DC of DF in 0–10 cm was 86.8 ± 6%, which was significantly greater than CF (60.0 ± 18%) ($p < 0.05$) under large rainfall event. However, the mean DC of CF (29.9 ± 14%) in 20–40 cm was significantly larger than that of DF (11.4 ± 4%) under extreme rainfall event ($p < 0.05$). At the DF site, mean maximum infiltration depth was 32.6 ± 5.8 cm and 36.3 ± 4.0 cm under large and extreme rainfall, respectively. For the CF site, mean maximum infiltration depth for the extreme rainfall was 38.3 ± 3.8 cm, which was significantly larger than that for the large rainfall ($p < 0.05$). Following the classification scheme of Weiler and Fluhler [57], the flow types in the soil profiles were determined based on the dye coverage of stained pathway widths (Figure 2). Macropore flow was the main flow type and accounted for 64.0–86.3% in the vertical soil profiles. No heterogeneous matrix flow was observed in CF-40 mm, and heterogeneous matrix flow and fingering were observed in DF-40, DF-70, and CF-70 mm.

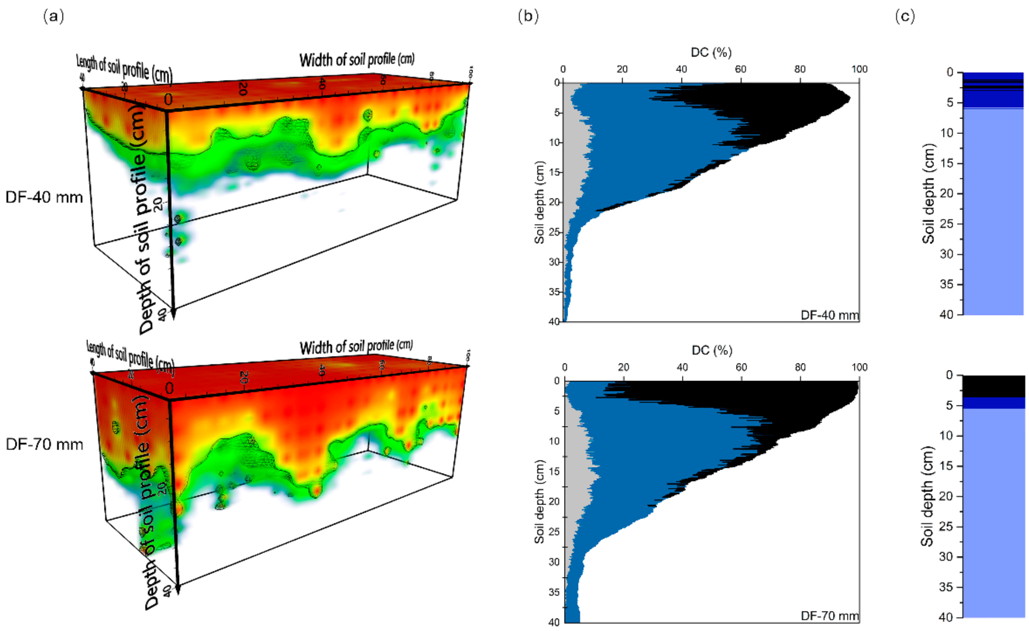

Figure 2. *Cont.*

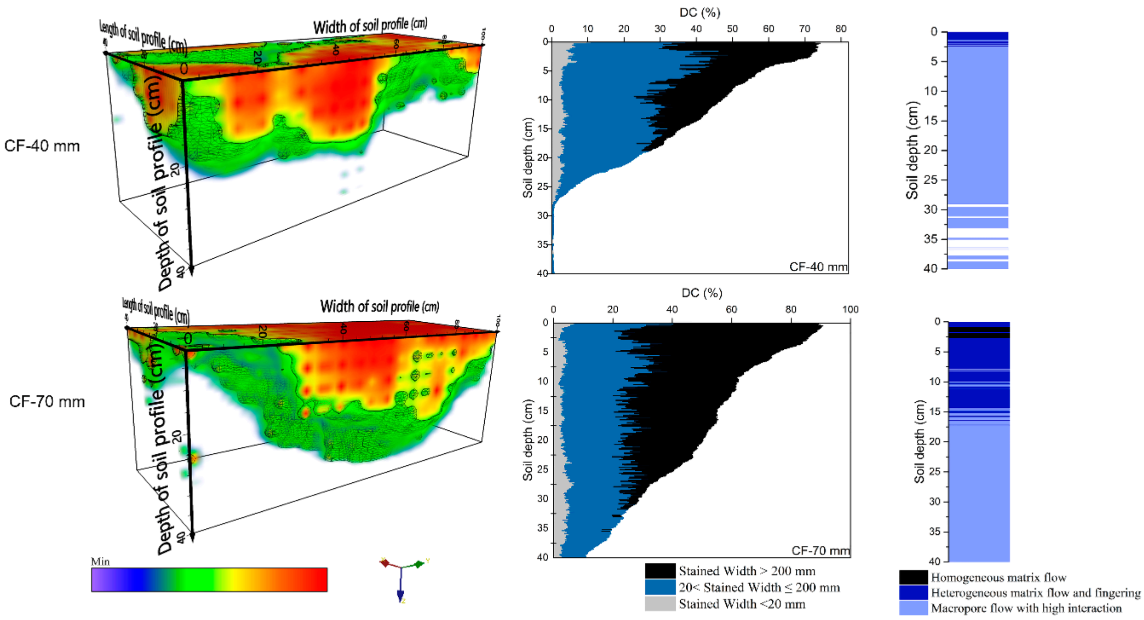

Figure 2. Characteristics of preferential flow (**a**) DC, (**b**) stained width distribution, and (**c**) preferential flow types) at DF and CF sites under large and extreme rainfall events. DF-40 and CF-40 mm were sampled for large rainfall (40 mm). DF-70 and CF-70 mm were sampled for extreme rainfall (70 mm). DF: deciduous forest; CF: coniferous forest; DC: dye coverage (%).

3.2. Spatial Variation of Preferential Flow Paths

The spatial distribution of DC at DF and CF are presented in Figure 3. The dye shows the transport paths of the preferential flow in the horizontal and vertical direction. Compared with CF, the horizontal distribution of DC at DF showed higher uniformity. In CF, high DC was observed in several scattered locations in the horizontal direction. In the vertical direction, a belt with high DC appeared in the range of 0–15 cm soil depth for both DF and CF. However, this belt was darker and less variable in DF as compared to CF. The corresponding semivariance parameters are summarized in Table 3. Exponential and gaussian models were fitted to the experimental semivariograms. The spatial autocorrelation range (A) that indicated the degree of horizontal and vertical similarity of DC was higher in CF than in DF. The $C_0/(C_0 + C)$ was less than 25% for DF and CF in horizontal and vertical (Table 3). This indicates that DC is strongly spatially dependent at all sites in both horizontal and vertical direction.

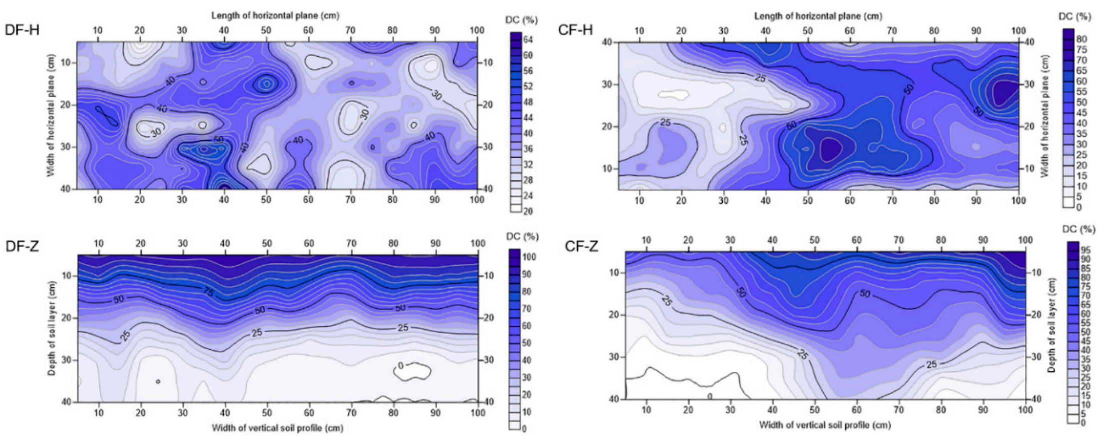

Figure 3. Spatial distribution of dye coverage (DC (%)). DF-H and CF-H are the horizontal spatial distribution of dye coverage in DF and CF, respectively; DF-Z and CF-Z are the vertical spatial distribution of dye coverage in DF and CF, respectively. DF: deciduous forest; CF: coniferous forest.

Table 3. Fitted parameters in the semi-variogram models for the dye coverage (DC, %) in horizontal and vertical planes of two types of forest sites.

Plane	Model	*A* (m)	C_0	$(C_0 + C)$	$C_0/(C_0 + C)$ (%)	Spatial Class	R^2	*RSS*
DF-H	E	0.27	0.0012	0.007	17.4	S	0.971	3.61×10^{-7}
DF-Z	G	0.38	0.0010	1.246	0.08	S	0.942	1.18×10^{-1}
CF-H	E	0.72	0.1360	1.286	10.6	S	0.960	2.85×10^{-2}
CF-Z	G	0.42	0.0001	0.153	0.07	S	0.971	8.44×10^{-4}

E: exponential model; G: gaussian model; *A*: spatial autocorrelation range; C_0: nugget variance; $(C_0 + C)$: sill; *S*: strong spatial dependence; R^2: coefficient of determination; *RSS*: residual sum of squares; DF-H and CF-H are the horizontal spatial distribution of dye coverage in DF and CF, respectively; DF-Z and CF-Z are the vertical spatial distribution of dye coverage in DF and CF, respectively. DF: deciduous forest; CF: coniferous forest.

3.3. Root Abundance (RA) in Vertical Soil Profile

Generally, the total *RA* decreased along soil depth for both DF and CF (Figure 4). More than 60% of total roots were found in the 0–20 cm soil layer for both sites. In the 0–10 cm soil layer, the mean total *RA* of DF (10.7/dm^2) was significantly larger than that of CF (9.6/dm^2) ($p < 0.05$). In the 20–40 cm soil layer, the mean total *RA* of CF was 5.71/dm^2, which was significantly larger than that of DF (4.84/dm^2) ($p < 0.05$). The roots with diameter < 5 mm for the 0–40 cm soil layer accounted for the largest proportion of *RA* (98.5 and 98.8% in DF and CF, respectively). Coarse roots (i.e., diameter > 5 mm) with less amount are mostly found in deeper soils (Figure 4). As shown in Figure 4, more than 50% of coarse roots accumulated in 20–40 cm soil layer for both sites.

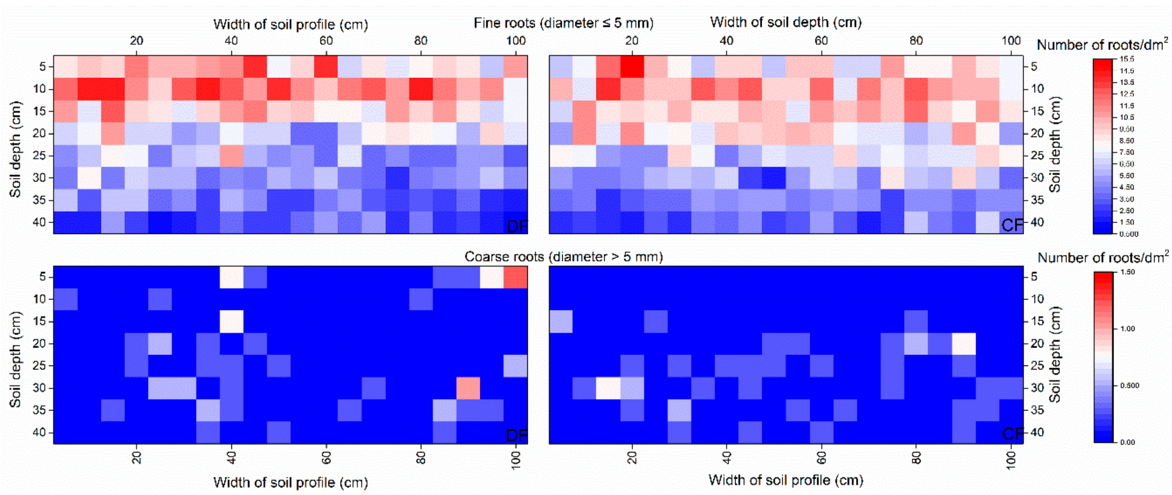

Figure 4. Root abundance (*RA*) of fine and coarse roots in soil profiles. DF: deciduous forest; CF: coniferous forest.

3.4. Variation of Root-Solute Interaction (RSI) in Forest Soils

Generally, the *RSI* decreased with soil depth in the 0–40 cm range (Figure 5). The *RSI* of DF was significantly larger than CF in the 0–20 cm soil layer ($p < 0.05$). However, there was no significant difference between DF and CF for the 20–40 cm soil layer ($p > 0.05$). In the 0–40 cm soil layer, *RSI* in subplots under extreme rainfall events was significantly larger than that under large rainfall events, especially for the 20–40 cm layer. There was a significant positive correlation between *RSI* and DC ($p < 0.01$). When DC = 0, the ratio of *RSI* > 0 was in the range 44.4%–64.6% for both sites. When DC > 0, mean *RSI* was 24 and 8 times higher than for DC = 0 in DF and CF, respectively.

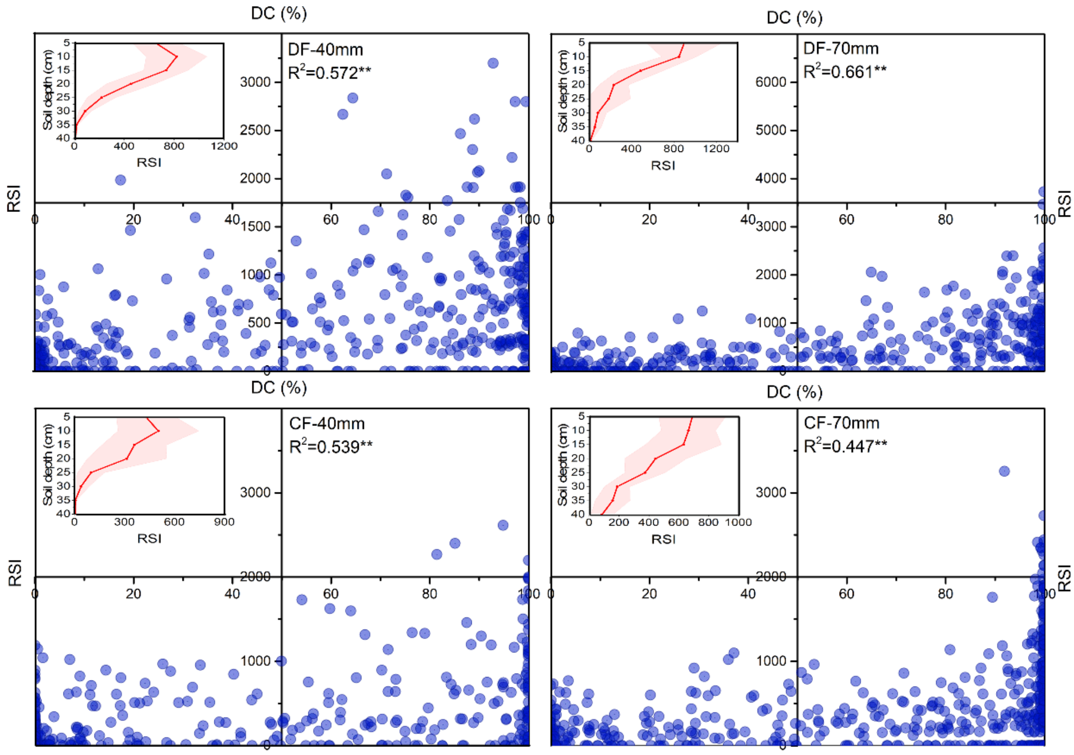

Figure 5. Features of root-solute interaction (*RSI*) in DF and CF soils. DF-40 and CF-40 mm are large rainfall event (40 mm). DF-70 and CF-70 mm are for extreme rainfall (70 mm). DF: deciduous forest; CF: coniferous forest.

4. Discussion

Dense and spatially variable structures of root systems in forest soils can result in well-developed pore systems with considerable influence on water and solute movement [3,26,31]. Deep and continuous stained pathways gradually decreased with soil depth and can be associated with root occurrence at the DF and CF sites (Figures 2–4) [64,65]. Most roots accumulated in the upper soil layers where preferential flow was frequent and *RSI* strong (Figures 2, 4 and 5). This is consistent studies by Ferchaud et al. and Dupont et al. [66,67]. Many studies have reported that roots generate preferential flow paths for water and solutes [25,68,69]. Principal preferential flow paths constituted by root channels can remain in function for decades and thus, lead water and solutes through the entire soil profile in forest ecosystems [70]. Our results showed that preferential flow paths at the DF and CF sites efficiently enhance infiltration during rainfall events (Figure 2). In general, macropore flow with high interaction between with the surrounding soil matrix was dominant through the entire forest soil profiles (Figure 2). Thus, our results concur with those of Alaoui et al. [70], and can be attributed to the prevalence of well-connected and stable macropores [71]. Yan et al. [43] found that soil structure is a critical factor that controls preferential flow pattern during large and extreme rainfall events. The different characteristics of preferential flow paths under large and extreme rainfall events indicate that, tree species with different root distribution can exert different influence on preferential flow. Compared to the CF site, accumulated roots in 0–10 cm soil layer of the DF enhanced the infiltration by lateral flow that resulted in large dye stained areas (Figures 2 and 4). During extreme rainfall events, CF soils transported more water and solutes in deeper soil layers as compared to DF soils (Figures 2 and 4). These results can be explained by the connectivity of macropore channels constituted by root structures. Abundant roots in the upper soil layer can reduce macropore connectivity, and impede the vertical infiltration movement in DF soils [21,38,39]. In our study, higher bulk density was found in 20–40 cm than in 0–20 cm soil layer in DF. This compact soil layer can as well impede the downward movement of water and solutes [72] (Figure 2). The larger spatial variability of preferential flow paths found in CF soils in both vertical and horizontal direction (Figure 3 and Table 3). These results are in agreement with our earlier observations, which showed that the degree of preferential flow is greater in CF soils as compared to DF soils [44]. As mentioned in the literature review, preferential flow can induce fast and deep downward movement of water and solutes [6,14,73]. Hence, CF soils were more efficient in water drainage, reducing surface runoff, and enhancing the infiltration as compared to DF soils during rainfall events in our study area.

Fine and coarse roots can change the size distribution and connectivity of soil pores, and affect the preferential infiltration process. In our study, the fine roots, that accounted for more than 90% to total roots in the entire soil profile, were the principal and most important factors for preferential flow at both sites (Figure 4). These results are supported by previous observations [74,75]. These studies reported that about 80% of fine roots were found in the upper 40–45 cm of the soil profile. The larger amount of fine roots can provide greater interfaces of roots and soil contact, and form interconnected networks that contribute to water percolation [76]. The rhizosphere increases organic matter content around the fine roots by the exudates from microorganisms and plant roots, which enhance soil aggregation and affect the occurrence of preferential flow [21,23]. Additionally, fine roots can enlarge the spaces between root and soil through emitting exudates, and facilitate the water and solute preferential transport [21,26]. Fine roots that are susceptible to soil dryness can form gaps between root and the soil by root shrinkage, and lead water flow rapidly from the ground surface to deeper soil layers [21,77]. On the other hand, fast turnover rate of fine roots would generate a number of well-connected void channels, which may provide new space for water and air storage [21,64]. Additionally, organic remains of root material and active microbial populations can improve the circumstances for macropores. These channels can also provide paths for new fine root growth with small mechanical resistance and high availability of water, air, and nutrients [21,78]. In our study, coarse roots seem to play a small role (less than 10% of total root occurrence for the entire soil profile; Figure 4). These coarse roots were mainly found at 20–40 cm soil depth, which in agreement with the study of Jost et al. [79]. Coarse roots can expand the diameter of root channels by root physical action, and enhance water penetration [21,80]. However, this kind of effect appears small in our study area. Hence, the fine roots contributed more to water and solute preferential transport than coarse roots in our study.

Preferential flow can enhance water and solute transport (Figure 5), which is in agreement with the results by Bogner et al., Brevik et al. and Singh et al. [12,24,81]. Our study demonstrated that higher *RSI* was found in preferential flow paths (DC > 0) than in the soil matrix (DC = 0) for both sites (Figure 5), which matches the observations of Zhang et al. [26]. Lipsius et al. [82] pointed out that preferential flow paths can impede effective absorbing and buffering capacity of the soil and reduce the residence time of solutes. Compared with the soil matrix, the proportion of living or decayed roots was greater in preferential flow paths [25]. When DC is larger than 0, the *RSI* was equal to 0 in the preferential flow (Figure 5). It is possible that other macropores formed by cracks or rock fragments may enhance the water and solute preferential penetration. In our study, intense interaction between roots and solute also occurred in the soil matrix (DC = 0) (Figure 5). These results are in agreement with the study of Wu et al. [83], who reported that plant roots can contribute to matrix flow mechanics, and influence the soil water infiltration. Our study, however, highlighted the importance of preferential flow in root-solute interaction for forest soils.

Dead root channels provide inter-connections among root systems, and can more efficiently generate preferential flow paths than living roots [25]. However, the distribution features of dead roots or decayed roots were not observed in our study, as it is difficult to define dead roots in field soil profiles [54,84]. Moreover, characteristics of soil layers can significantly influence the water movement [85]. Flow pathways can be described by a mixture of roots and stones in rocky mountainous areas [26]. Our study, however, did not consider these processes since number of observed rocks and stones is low for the study sites. Further field studies may, however, use ground penetrating radar to nondestructively obtain more information about rock fragments in soil layers [86].

5. Conclusions

In this study, root abundance characteristics, preferential flow path features, and solute concentration were investigated in soil profiles. We analyzed the effects of root distribution (fine and coarse roots) on water and solute transport in forest soils by dual-tracer experiments under large and extreme rainfall events. Our study indicated that root-enhanced preferential flow paths observed in deciduous and coniferous forest soils can exert different effects on the movement of the water and solutes during different rainfall events. Preferential flow paths can facilitate the water and solute movement during rainfall events. Compared to coniferous forest soils, deciduous forest soils with abundant roots in the upper soil layer has a more positive impact on increasing infiltration and reducing surface runoff by lateral preferential flow. During extreme rainfall events, coniferous forest soil with higher (horizontal and vertical) spatial variability of preferential flow paths than deciduous forest, can promote more water percolation and solute leaching to deeper soil layers than in deciduous forests. Compared to coarse roots, fine roots more significantly affect the preferential flow in the 0–40 cm forest soil during rainfall events. Thus, our study highlighted the effects of different root distribution (fine and coarse roots) on preferential flow for the different tree species.

Author Contributions: Conceptualization, Z.L., J.N., and R.B.; Funding acquisition, J.N.; Investigation, Z.L., J.N., B.X., L.Z., X.C., J.D., J.A., L.Y., and S.Z.; Methodology, Z.L. and J.N.; Project administration, J.N.; Supervision, J.N., B.X., L.Z., and X.C.; Writing—original draft, Z.L. and J.N.; Writing—review & editing, B.X., L.Z., X.C. and R.B.

Funding: This study was supported by the National Natural Science Foundation of China (No. 41877154), the National Natural Science Foundation of China (No. 41741024), and grants from the Beijing Municipal Education Commission (No. CEFF-PXM2018_014207_000024). USDA Mc-Stennis (1008643) and Shaoxing330. The Graduate Training and Development Program of Beijing Municipal Commission of Education (BLCXY201623).

Conflicts of Interest: The authors declare no conflicts of interest.

References

1. Mei, X.; Zhu, Q.; Ma, L.; Zhang, D.; Wang, Y.; Hao, W. Effect of stand origin and slope position on infiltration pattern and preferential flow on a Loess hillslope. *Land Degrad. Dev.* **2018**, *29*, 1353–1365. [CrossRef]
2. Köhne, J.M.; Köhne, S.; Šimůnek, J. A review of model applications for structured soils: a) Water flow and tracer transport. *J. Contam. Hydrol.* **2009**, *104*, 4–35. [CrossRef] [PubMed]
3. Jarvis, N.J. A review of non-equilibrium water flow and solute transport in soil macropores: Principles, controlling factors, and consequences for water quality. *Eur. J. Soil Sci.* **2007**, *58*, 523–546. [CrossRef]
4. Julich, D.; Julich, S.; Feger, K.H. Phosphorus in preferential flow pathways of forest soils in Germany. *Forests* **2017**, *8*, 19. [CrossRef]
5. Julich, S.; Benning, R.; Julich, D.; Feger, K. Quantification of phosphorus exports from a small forested headwater-catchment in the Eastern Ore Mountains, Germany. *Forests* **2017**, *8*, 206. [CrossRef]
6. Beven, K.; Germann, P.E. Macropores and water flow in soils revisited. *Water Resour. Res.* **2013**, *6*, 3071–3092. [CrossRef]
7. Sheng, F.; Wang, K.; Zhang, R.; Liu, H. Modeling preferential water flow and solute transport in unsaturated soil using the active region model. *Environ. Earth Sci.* **2011**, *62*, 1491–1501. [CrossRef]
8. Clothier, B.; Green, S.R.; Deurer, M. Preferential flow and transport in soil: Progress and prognosis. *Eur. J. Soil Sci.* **2008**, *59*, 2–13. [CrossRef]
9. Darnault, C.J.G.; Steenhuis, T.S.; Garnier, P.; Kim, Y.J.; Jenkins, M.; Ghiorse, W.C.; Baveye, P.; Parlange, J.Y. Preferential Flow and Transport of Cryptosporidium parvum Oocysts through the Vadose Zone: Experiments and Modeling. *Vadose Zone J.* **2004**, *3*, 262–270. [CrossRef]
10. Stamm, C.; Flühler, H.; Gächter, R.; Leuenberger, J.; Wunderli, H. Preferential Transport of Phosphorus in Drained Grassland Soils. *J. Environ. Qual.* **1998**, *27*, 515–522. [CrossRef]
11. Jiang, X.J.; Liu, W.J.; Chen, C.F.; Liu, J.Q.; Yuan, Z.Q.; Jin, B.C.; Yu, X.Y. Effects of three morphometric features of roots on soil water flow behavior in three sites in China. *Geoderma* **2018**, *320*, 161–171. [CrossRef]
12. Bogner, C.; Gaul, D.; Kolb, A.; Schmiedinger, I.; Huwe, B. Analysing flow patterns from dye tracer experiments in a forest soil using extreme value statistics. *Eur. J. Soil Sci.* **2010**, *61*, 1079–1090. [CrossRef]

13. Gerke, H.H. Preferential flow descriptions for structured soils. *J. Plant Nutr. Soil Sci.* **2006**, *169*, 382–400. [CrossRef]
14. Hendrickx, J.M.; Flury, M. Uniform and preferential flow mechanisms in the vadose zone. In *Conceptual Models of Flow and Transport in the Fractured Vadose Zone*; National Research Council, Ed.; National Academy Press: Washington, DC, USA, 2001; pp. 149–187.
15. Zehe, E.; Flühle, H. Preferential transport of isoproturon at a plot scale and a field scale tile-drained site. *J. Hydrol.* **2001**, *247*, 100–115. [CrossRef]
16. Schwen, A.; Backus, J.; Yang, Y.; Wendroth, O. Characterizing land use impact on multi-tracer displacement and soil structure. *J. Hydrol.* **2014**, *519*, 1752–1768. [CrossRef]
17. Newman, B.D.; Wilcox, B.P.; Graham, R.C. Snowmelt-driven macropore flow and soil saturation in a semiarid forest. *Hydrol. Proc.* **2004**, *18*, 1035–1042. [CrossRef]
18. Noguchi, S.; Tsuboyama, Y.; Sidle, R.C.; Hosoda, L. Spatially distributed morphological characteristics of macropores in forest soils of Hitachi Ohta experimental watershed. *Jpn. J. For. Res.* **1997**, *2*, 207–215. [CrossRef]
19. Dusek, J.; Vogel, T.; Lichner, L.; Čipáková, A.; Dohnal, M. Simulated cadmium transport in macroporous soil during heavy rainstorm using dual-permeability approach. *Biologia* **2006**, *61*, S251–S254. [CrossRef]
20. Jørgensen, P.R.; Hoffmann, M.; Kistrup, J.P.; Bryde, C.; Bossi, R.; Villholth, K.G. Preferential flow and pesticide transport in a clay-rich till: Field, laboratory, and modeling analysis. *Water Resour. Res.* **2002**, *38*, 1246–1261. [CrossRef]
21. Ghestem, M.; Sidle, R.C.; Stokes, A. The influence of plant root systems on subsurface flow: Implications for slope stability. *Bioscience* **2011**, *61*, 869–879. [CrossRef]
22. Vannoppen, W.; Vanmaercke, M.; De Baets, S.; Poesen, J. A review of the mechanical effects of plant roots on concentrated flow erosion rates. *Earth Sci. Rev.* **2015**, *150*, 666–678. [CrossRef]
23. Fageria, N.K.; Stone, L.F. Physical, Chemical, and Biological Changes in the Rhizosphere and Nutrient Availability. *J. Plant Nutr.* **2006**, *29*, 1327–1356. [CrossRef]
24. Singh, Y.P.; Nayak, A.K.; Sharma, D.K.; Singh, G.; Mishra, V.K.; Singh, D. Evaluation of Jatropha curcas genotypes for rehabilitation of degraded. *Land Degrad. Dev.* **2015**, *26*, 510–520. [CrossRef]
25. Zhang, Y.H.; Niu, J.Z.; Yu, X.X.; Zhu, W.L.; Du, X.Q. Effects of fine root length density and root biomass on soil preferential flow in forest ecosystems. *For. Syst.* **2015**, *24*, 12. [CrossRef]
26. Zhang, Y.; Niu, J.; Zhang, M.; Xiao, Z.; Zhu, W. Interaction Between Plant Roots and Soil Water Flow in Response to Preferential Flow Paths in Northern China. *Land Degrad. Dev.* **2016**, *28*, 648–663. [CrossRef]
27. Blevins, R.L.; Holowaychuk, N.; Wilding, L.P. Micromorphology of soil fabric at tree root-soil interface. *Soil Sci. Soc. Am. J.* **1970**, *34*, 460–465. [CrossRef]
28. Guo, L.; Gregory, J.M.; Sean, H.; Henry, L.; Delphis, L. Pairing geophysical techniques improves understanding of the near-surface Critical Zone: Visualization of preferential routing of stemflow along coarse roots. *Geoderma* **2020**, *357*, 113953. [CrossRef]
29. Uchida, T.; Kosugi, K.; Mizuyama, T. Effects of pipeflow on hydrological process and its relation to landslide: A review of pipeflow studies in forested headwater catchments. *Hydrol. Process.* **2001**, *15*, 2151–2174. [CrossRef]
30. Sidle, R.C.; Tsuboyama, Y.; Noguchi, S.; Hosoda, I.; Fujieda, M.; Shimizu, T. Stormflow generation in steep forested headwaters: A linked hydrogeomorphic paradigm. *Hydrol. Process.* **2000**, *14*, 369–385. [CrossRef]
31. Legout, A.; Legout, C.; Nys, C.; Dambrine, E. Preferential flow and slow convective chloride transport through the soil of a forested landscape (Fougères, France). *Geoderma* **2009**, *151*, 179–190. [CrossRef]
32. Beven, K.; Germann, P.F. Macropores and water flow in soils. *Water Resour. Res.* **1982**, *18*, 1311–1325. [CrossRef]
33. Backnäs, S.; Laine-Kaulio, H.; Kløve, B. Phosphorus forms and related soil chemistry in preferential flow paths and the soil matrix of a forested podzolic till soil profile. *Geoderma* **2012**, *189*, 50–64. [CrossRef]
34. Bargués Tobella, A.; Reese, H.; Almaw, A.; Bayala, J.; Malmer, A.; Laudon, H.; Llstedt, U. The effect of trees on preferential flow and soil infiltrability in an agroforestry parkland in semiarid Burkina Faso. *Water Resour. Res.* **2014**, *50*, 3342–3354. [CrossRef] [PubMed]

35. Ceccon, C.; Panzacchi, P.; Scandellari, F.; Prandi, L.; Ventura, M.; Russo, B.; Millard, P.; Tagliavini, M. Spatial and temporal effects of soil temperature and moisture and the relation to fine root density on root and soil respiration in a mature apple orchard. *Plant Soil* **2011**, *342*, 195–206. [CrossRef]
36. Laine-Kaulio, H.; Backnäs, S.; Koivusalo, H.; Laurén, A. Dye tracer visualization of flow patterns and pathways in glacial sandy till at a boreal forest hillslope. *Geoderma* **2015**, *259*, 23–34. [CrossRef]
37. Keesstra, S.; Pereira, P.; Novara, A.; Brevik, E.C.; Azorin-Molina, C.; Parras-Alcántara, L.; Jordán, A.; Cerdà, A. Effects of soil management techniques on soil water erosion in apricot orchards. *Sci. Total Environ.* **2016**, *551*, 357–366. [CrossRef]
38. Liu, M.; Guo, L.; Yi, J.; Lin, H.; Luo, S.; Zhang, H.; Li, T. Characterising preferential flow and its interaction with the soil matrix using dye tracing in the Three Gorges Reservoir Area of China. *Soil Res.* **2018**, *56*, 588–600. [CrossRef]
39. Jia, G.; Liu, Z.; Chen, L.; Yu, X. Distinguish water utilization strategies of trees growing on earth-rocky mountainous area with transpiration and water isotopes. *Ecol. Evol.* **2017**, *7*, 10640–10651. [CrossRef]
40. Bauhus, J.; Messier, C. Soil exploitation strategies of fine roots in different tree species of the southern boreal forest of eastern Canada. *Can. J. For. Res.* **1999**, *29*, 260–273. [CrossRef]
41. Liu, Z.; Yu, X.; Jia, G. Water uptake by coniferous and broad-leaved forest in a rocky mountainous area of northern China. *Agric. For. Meteorol.* **2019**, *265*, 381–389. [CrossRef]
42. Jia, J.B.; Yu, X.X.; Li, Y.T. Response of forestland soil water content to heavy rainfall on Beijing Mountain, northern China. *J. For. Res.* **2016**, *27*, 541–550. [CrossRef]
43. Yan, J.; Zhao, W. Characteristics of preferential flow during simulated rainfall events in an arid region of China. *Environ. Earth Sci.* **2016**, *75*, 566. [CrossRef]
44. Luo, Z.; Niu, J.; Zhang, L.; Chen, X.; Zhang, W.; Xie, B.; Du, J.; Zhu, Z.; Wu, S.; Li, X. Roots-Enhanced Preferential Flows in Deciduous and Coniferous Forest Soils Revealed by Dual-Tracer Experiments. *J. Environ. Qual.* **2019**, *48*, 136–146. [CrossRef] [PubMed]
45. Wang, K.; Zhang, R. Heterogeneous soil water flow and macropores described with combined tracers of dye and iodine. *J. Hydrol.* **2011**, *397*, 105–117. [CrossRef]
46. Janssen, M.; Lennartz, B. Characterization of preferential flow pathways through paddy bunds with dye tracer tests. *Soil Sci. Soc. Am. J.* **2008**, *72*, 1756–1766. [CrossRef]
47. Sheng, F.; Liu, H.; Wang, K.; Zhang, R.; Tang, Z. Investigation into preferential flow in natural unsaturated soils with field multiple-tracer infiltration experiments and the active region model. *J. Hydrol.* **2014**, *508*, 137–146. [CrossRef]
48. Flury, M.; Wai, N.N. Dyes as tracers for vadose zone hydrology. *Rev. Geophys.* **2003**, *41*, 1002. [CrossRef]
49. Li, X.; Niu, J.; Zhang, L.; Xiao, Q.; McPherson, G.E.; van Doorn, N.; Meng, C. A study on crown interception with four dominant tree species: A direct measurement. *Hydrol. Res.* **2016**, *47*, 857–868. [CrossRef]
50. Bachmair, S.; Weiler, M.; Nützmann, G. Controls of land use and soil structure on water movement: Lessons for pollutant transfer through the unsaturated zone. *J. Hydrol.* **2009**, *369*, 241–252. [CrossRef]
51. Finér, L.; Ohashi, M.; Noguchi, K.; Hirano, Y. Fine root production and turnover in forest ecosystems in relation to stand and environmental characteristics. *For. Ecol. Manag.* **2011**, *262*, 2008–2023. [CrossRef]
52. Kurz, W.A.; Beukema, S.J.; Apps, M.J. Estimation of root biomass and dynamics for the carbon budget model of the Canadian forest sector. *Can. J. For. Res.* **1996**, *26*, 1973–1979. [CrossRef]
53. Vanlauwe, B.; Akinnifesi, F.K.; Tossah, B.K.; Lyasse, O.; Sanginga, N.; Merckx, R. Root distribution of Senna siamea grown on a series of derived-savanna-zone soils in Togo, West Africa. *Agrofor. Syst.* **2002**, *54*, 1–12. [CrossRef]
54. Van Noordwijk, M.; Brouwer, G.; Meijboom, F.; do Rosario, M.; Oliveira, G.; Bengough, A.G. Trench Profile Techniques and Core Break Methods. In *Root Methods: A Handbook*; Smit, A.L., Bengough, A.G., Engels, C., Noordwijk, M., Pellerin, S., Geijn, S.C., Eds.; Springer: Berlin, Germany, 2000; pp. 211–223.
55. Koch, S.; Kahle, P.; Lennartz, B. Visualization of Colloid Transport Pathways in Mineral Soils Using Titanium(IV) Oxide as a Tracer. *J. Environ. Qual.* **2016**, *45*, 2053–2059. [CrossRef] [PubMed]
56. Nobles, M.M.; Wilding, L.P.; Lin, H.S. Flow pathways of bromide and Brilliant Blue FCF tracers in caliche soils. *J. Hydrol.* **2010**, *393*, 114–122. [CrossRef]
57. Weiler, M.; Flühler, H. Inferring flow types from dye patterns in macroporous soils. *Geoderma* **2004**, *120*, 137–153. [CrossRef]

58. Jiang, X.; Liu, X.; Wang, E.; Li, X.; Sun, R.; Shi, W. Effects of tillage pan on soil water distribution in alfalfa-corn crop rotation systems using a dye tracer and geostatistical methods. *Soil Tillage Res.* **2015**, *150*, 68–77. [CrossRef]
59. Zhou, J.; Feng, K.; Pei, Z.; Lu, M. Pollution assessment and spatial variation of soil heavy metals in Lixia River Region of Eastern China. *J. Soils Sediments* **2016**, *16*, 748–755. [CrossRef]
60. Fu, W.; Tunney, H.; Zhang, C. Spatial variation of soil nutrients in a dairy farm and its implications for site-specific fertilizer application. *Soil Tillage Res.* **2010**, *106*, 185–193. [CrossRef]
61. Liu, H.; Lennartz, B. Visualization of Flow Pathways in Degraded Peat Soils Using Titanium Dioxide. *Soil Sci. Soc. Am. J.* **2015**, *79*, 757–765. [CrossRef]
62. Daigle, A.; St-Hilaire, A.; Peters, D.; Baird, D. Multivariate Modelling of Water Temperature in the Okanagan Watershed. *Can. Water Resour. J.* **2010**, *35*, 237–258. [CrossRef]
63. Casado, M.R.; Parsons, D.J.; Magan, N.; Weightman, R.M.; Battilani, P.; Poetri, A. A short geostatistical study of the three-dimensional spatial structure of fumonisins in maize. *World Mycotoxin J.* **2010**, *3*, 95–103. [CrossRef]
64. Guo, L.; Liu, Y.; Wu, G.; Huang, Z.; Cui, Z.; Cheng, Z.; Zhang, R.; Tian, F.; He, H. Preferential water flow: Influence of alfalfa (*Medicago sativa* L.) decayed root channels on soil water infiltration. *J. Hydrol.* **2019**, *578*, 124019. [CrossRef]
65. Devitt, D.A.; Smith, S.D. Root channel macropores enhance downward movement of water in a Mojave Desert ecosystem. *J. Arid Environ.* **2002**, *50*, 99–108. [CrossRef]
66. Ferchaud, F.; Vitte, G.; Bornet, F.; Strullu, L.; Mary, B. Soil water uptake and root distribution of different perennial and annual bioenergy crops. *Plant Soil* **2015**, *388*, 307–322. [CrossRef]
67. DuPont, S.T.; Beniston, J.; Glover, J.D.; Hodson, A.; Culman, S.W.; Lal, R.; Ferris, H. Root traits and soil properties in harvested perennial grassland, annual wheat, and never-tilled annual wheat. *Plant Soil* **2014**, *381*, 405–420. [CrossRef]
68. Tracy, S.R.; Black, C.R.; Roberts, J.A.; Mooney, S.J. Exploring the interacting effect of soil texture and bulk density on root system development in tomato (*Solanum lycopersicum* L.). *Environ. Exp. Bot.* **2013**, *91*, 38–47. [CrossRef]
69. Bengough, A.G. Water Dynamics of the Root Zone: Rhizosphere Biophysics and Its Control on Soil Hydrology. *Vadose Zone J.* **2012**, 11. [CrossRef]
70. Alaoui, A.; Caduff, U.; Gerke, H.H.; Weingartner, R. A preferential flow effects on infiltration and runoff in grassland and forest soils. *Vadose Zone J.* **2011**, *10*, 367–377. [CrossRef]
71. Meng, C.; Niu, J.; Li, X.; Luo, Z.; Du, X.; Du, J.; Lin, X.; Yu, X. Quantifying soil macropore networks in different forest communities using industrial computed tomography in a mountainous area of North China. *J. Soils Sediments* **2018**, *17*, 2357–2370. [CrossRef]
72. Morales, V.L.; Parlange, J.Y.; Steenhuis, T.S. Are preferential flow paths perpetuated by microbial activity in the soil matrix? A review. *J. Hydrol.* **2010**, *393*, 29–36. [CrossRef]
73. Allaire, S.E.; Roulier, S.; Cessna, A.J. Quantifying preferential flow in soils: A review of different techniques. *J. Hydrol.* **2009**, *378*, 179–204. [CrossRef]
74. Crow, P.; Houston, T.J. The influence of soil and coppice cycle on rooting habit of short rotation poplar and willow coppice. *Biomass Bioenergy* **2004**, *26*, 497–505. [CrossRef]
75. Rytter, R.M.; Hansson, A.C. Seasonal amount, growth and depth distribution of fine roots in an irrigated and fetilized *Salix viminalis* L. *Biomass Bioenergy* **1996**, *11*, 129–137. [CrossRef]
76. Sidle, R.C.; Noguchi, S.; Tsuboyama, Y.; Laursen, K. A conceptual model of preferential flow systems in forested hillslopes: Evidence of self-organization. *Hydrol. Process.* **2001**, *15*, 1675–1692. [CrossRef]
77. DeRoo, H.C. Tillage and root growth. In *Root Growth*; Whittington, W.J., Ed.; Butterworths: London, UK, 1968; pp. 339–358.
78. Jassogne, L.; McNeill, A.; Chittleborough, D. 3D-visualization and analysis of macro- and meso-porosity of the upper horizons of a sodic, texture-contrast soil. *Eur. J. Soil Sci.* **2007**, *58*, 589–598. [CrossRef]
79. Jost, G.; Schume, H.; Hager, H.; Markart, G.; Kohl, B. A hillslope scale comparison of tree species influence on soil moisture dynamics and runoff processes during intense rainfall. *J. Hydrol.* **2012**, *420*, 112–124. [CrossRef]
80. Bodner, G.; Leitner, D.; Kaul, H.P. Coarse and fine root plants affect pore size distributions differently. *Plant Soil* **2014**, *380*, 133–151. [CrossRef]

81. Brevik, E.C.; Cerdà, A.; Mataix-Solera, J.; Pereg, L.; Quinton, J.N.; Six, J.; Van Oost, K. The interdisciplinary nature of SOIL. *Soil* **2015**, *1*, 117–129. [CrossRef]
82. Lipsius, K.; Mooney, S.J. Using image analysis of tracer staining to examine the infiltration patterns in a water repellent contaminated sandy soil. *Geoderma* **2006**, *136*, 865–875. [CrossRef]
83. Wu, G.; Liu, Y.; Yang, Z.; Cui, Z.; Deng, L.; Chang, X.; Shi, Z. Root channels to indicate the increase in soil matrix water infiltration capacity of arid reclaimed mine soils. *J. Hydrol.* **2017**, *546*, 133–139. [CrossRef]
84. Sierra, C.A.; Del Valle, J.I.; Orrego, S.A. Accounting for fine root mass sample losses in the washing process: A case study from a tropical Montane Forest of Colombia. *J. Trop. Ecol.* **2003**, *19*, 599–601. [CrossRef]
85. Zhang, J.; Lin, H.; Doolittle, J. Soil layering and preferential flow impacts on seasonal changes of GPR signals in two contrasting soils. *Geoderma* **2014**, *213*, 560–569. [CrossRef]
86. Poisson, J.; Chouteau, M.; Aubertin, M.; Campos, D. Geophysical experiments to image the shallow internal structure and the moisture distribution of a mine waste rock pile. *J. Appl. Geophys.* **2009**, *67*, 179–192. [CrossRef]

© 2019 by the authors. Licensee MDPI, Basel, Switzerland. This article is an open access article distributed under the terms and conditions of the Creative Commons Attribution (CC BY) license (http://creativecommons.org/licenses/by/4.0/).